SLAC–PUB–7741
January 1998

Final-Focus System and Collision Schemes for a 5-TeV W-Band Linear Collider*

F. Zimmermann and D.H. Whittum
Stanford Linear Accelerator Center, Stanford University, California 94309

A 3-km long high-gradient W-band switched matrix linac may, in parallel channels, accelerate multiple electron and positron bunches to an energy of 2.5 TeV, with a tight control on the intra-bunch energy spread. In this report, we describe a final-focus system for such an accelerator, whose length is restrained by eliminating chromatic correction. The interaction point (IP) spot size is limited by synchrotron radiation in the last quadrupole (Oide effect). The energy loss due to beamstrahlung is optionally suppressed by combining bunches of opposite charge and colliding the neutral beams. We present two different high-luminosity multiple-collision schemes, which can provide a luminosity of up to 10^{35} cm^{-2} s^{-1}, with only about 1 MW average beam power. In the first scheme, batches of equally-charged bunches are combined into superbunches which, possibly after charge compensation, are collided head-on with the opposing beam. In the second scheme, 25 charge-neutral electron-positron bunch pairs of one beam are each collided with 25 neutral bunch pairs of the other beam. These multiplexed collisions are facilitated by a crossing angle and by crab cavities upstream of the electron-positron combiner; however they also require focusing channels (*e.g.*, a crystal) preserving the IP beam size between the collision points, a difficult if not impossible construct. We describe the challenges posed by each approach.

Invited Talk at the Second International Workshop on Electron-Electron Interactions at TeV Energies
Santa Cruz, California, September 22–24, 1997

*Work supported by the U.S. Department of Energy under the Contract No. DE-AC03-76SF00515.

FINAL-FOCUS SYSTEM AND COLLISION SCHEMES FOR A 5-TeV W-BAND LINEAR COLLIDER*

F. ZIMMERMANN and D.H. WHITTUM
Stanford Linear Accelerator Center, Stanford University, CA 94309

A 3-km long high-gradient W-band switched matrix linac may, in parallel channels, accelerate multiple electron and positron bunches to an energy of 2.5 TeV, with a tight control on the intra-bunch energy spread. In this report, we describe a final-focus system for such an accelerator, whose length is restrained by eliminating chromatic correction. The interaction point (IP) spot size is limited by synchrotron radiation in the last quadrupole (Oide effect). The energy loss due to beamstrahlung is optionally suppressed by combining bunches of opposite charge and colliding the neutral beams. We present two different high-luminosity multiple-collision schemes, which can provide a luminosity of up to 10^{35} cm^{-2} s^{-1}, with only about 1 MW average beam power. In the first scheme, batches of equally-charged bunches are combined into superbunches which, possibly after charge compensation, are collided head-on with the opposing beam. In the second scheme, 25 charge-neutral electron-positron bunch pairs of one beam are each collided with 25 neutral bunch pairs of the other beam. These multiplexed collisions are facilitated by a crossing angle and by crab cavities upstream of the electron-positron combiner; however they also require focusing channels (*e.g.*, a crystal) preserving the IP beam size between the collision points, a difficult if not impossible construct. We describe the challenges posed by each approach.

1. Introduction

In this section we introduce the W-band matrix linac and the characteristic properties of the beam it can provide, consider luminosity limitations at high energies, sketch two possible collision schemes suggested by the above, present a list of interaction-point beam parameters, and describe the contents of the remainder of the paper.

1.1. *Switched Matrix Accelerator*

A switched matrix linac, operating at 91 GHz (W-band), may accelerate multiple bunches with a loaded gradient of 1 GV/m, while confining the exposure time for single copper surfaces to a subnanosecond time interval. Such a matrix linac constitutes a very promising scheme for establishing multi-TeV e^+e^- or e^-e^- collisions. Each beam consists of batches of about 25 low-charge electron and positron bunches that are accelerated in an array of parallel channels, with a horizontal inter-channel spacing Δx of 1.4 mm. A schematic of the linac is shown in Fig. 1. The rf power is fed into the accelerating channels orthogonally to the direction of the beam propagation, giving rise to a matrix configuration.

*Work supported by the US Department of Energy under Contract DE-AC03-76SF00515.

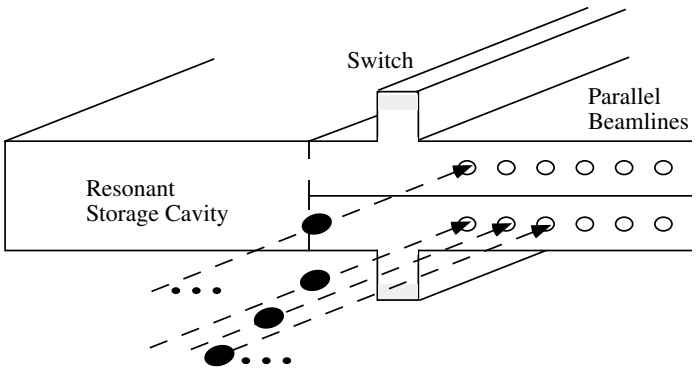

Fig. 1. A switched matrix linac consisting of 25 parallel positron beam lines, situated below 25 parallel electron beam lines.

The bunch-train pattern and the rf pulse for a matrix accelerator differ markedly from those in a conventional traveling-wave linac, as illustrated in Fig. 2. In a matrix linac, the total length T_p of the flat-top rf pulse is short, about 300 ps, which minimizes problems associated with pulsed heating. Since the bunches must pass through the accelerating structure at a moment when the rf wave is present, the permissible bunch-timing patterns are constrained as follows: For an rf group velocity v_g of $0.2c$, the maximum number of adjacent channels in which bunches can be accelerated without any time delay is $T_p v_g/(\Delta x) \approx 12$. On the other hand, the maximum time delay between two bunches of the same beam pulse is given by the transit time T_t of the rf pulse: Across a series of 50 parallel channels the transit time is about $T_t \approx 50\ \Delta x/v_g \approx 1$ ns. The total variation of the rf gradient over all accelerating channels, due to beam loading and rf-wave dispersion, is about 20%. The resulting bunch-to-bunch energy variation could be used, along with a half chicane, to combine groups of linac bunches into superbunches of higher charge, at the end of the linac. The energy variation across the bunch train could be reduced by tapering the iris radii.

We are considering two specific timing patterns which are optimized for two different multiple-collision schemes. These two timing patterns are depicted in Fig. 3. The first pattern of interest is a uniform time separation between adjacent electron-positron bunch pairs of about 25 ps, for a total of 2×25 bunches. In the second scheme, 2 batches consisting of 12 electron and 12 positron bunches each are accelerated with a batch-to-batch time separation of 300 ps and with equal arrival times for the bunches within a batch.

1.2. *Luminosity and Beamstrahlung*

The cross section for most high-energy physics reactions decreases roughly proportional to the inverse square of the c.m. energy, which suggests that the luminosity of a high-energy collider should increase as the square of the energy. Assuming that each bunch collides with n_{coll} bunches in the other train (for a conventional collider

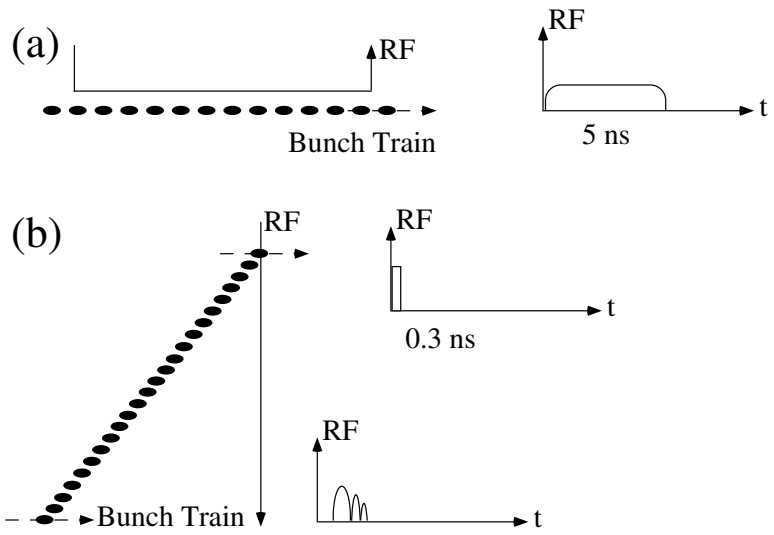

Fig. 2. Schematic of bunch trains and rf pulses: (a) in a conventional traveling-wave linac; (b) in a switched matrix accelerator.

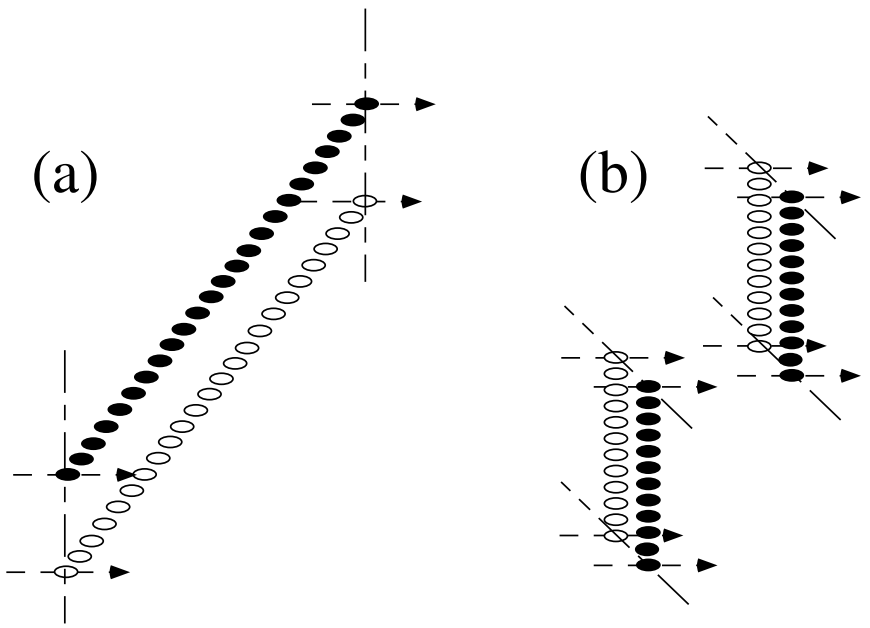

Fig. 3. Schematic of timing patterns for two different collision schemes: (a) for multiplexed collisions; (b) for cluster collisions. The black and open ellipses represent electron and positron bunches, respectively, which are later combined to form neutral beams.

$n_{coll} = 1$), the electron-positron luminosity can be written as

$$L_{e^+e^-} = n_{pair} \, \frac{n_b}{n_{coll}} \, \frac{f_{rep} N_b^2 n_{coll}^2}{4\pi\sigma_x\sigma_y} \, H_D \tag{1}$$

where f_{rep} denotes the repetition frequency, N_b the bunch population, n_b the number of bunches, and $\sigma_{x,y}$ the transverse rms beam size at the interaction point. The quantity n_{pair} is 1 for 2-beam collisions and equal to 2 for 4-beam collisions. The case of 4 beams corresponds to co-propagating electron and positron bunch pairs, which are combined into a single charge-neutral bunch at the IP ('charge compensation').[1,2] Finally, H_D is a factor which represents both luminosity enhancement due to beam-beam disruption and luminosity degradation from the hourglass effect. For the parameters of interest in this paper, $\sigma_z \ll \beta^*_{x,y}$, so that the hourglass effect is not important, and, if we also assume charge compensation, the factor H_D is very close to unity. In the case of charge-compensated 4-beam collisions, the electron-electron and positron-positron luminosities are of similar magnitude and equal to half the electron-positron luminosity: $L_{e^-e^-} \approx L_{e^+e^+} \approx L_{e^+e^-}/2$. Let us then define the total luminosity for 4-beam collisions as $L_{tot} \equiv 4L_{e^-e^-}$.

The motivation for charge compensation is beamstrahlung: During a collision, the beam particles can lose a significant amount of energy due to synchrotron radiation in the electromagnetic field of the opposing beam. It is customary to measure the field strength in terms of a dimensionless quantity Υ:

$$\Upsilon = \frac{5\gamma N_b r_e^2}{6\sigma_z(\sigma_x + \sigma_y)\alpha} \tag{2}$$

where $\alpha \approx 1/137$ is the fine structure constant, r_e the classical electron radius, and σ_z the rms bunch length. The number of photons emitted per electron and per collision, written in terms of Υ, is approximately[3]

$$N_\gamma \approx \frac{5}{2} \, \frac{\alpha\sigma_z}{\gamma\lambda\!\!\!^{-}_c} \, \frac{\Upsilon}{\sqrt{1+\Upsilon^{2/3}}} \tag{3}$$

with $\lambda\!\!\!^{-}_c$ the Compton wavelength, and the average energy loss per electron and per collision reads[3]

$$\delta_b^{coll} \approx \frac{1}{2} \, N_\gamma \Upsilon \frac{(1+\Upsilon^{2/3})^{1/2}}{\left(1+\left(\frac{3}{2}\Upsilon\right)^{2/3}\right)^2}. \tag{4}$$

For small δ_b^{coll}, the average energy loss after n_{coll} collisions is simply $\delta_b^{tot} \approx n_{coll}\delta_b^{coll}$. Hence, this energy spread increases linearly with the number of collisions, while, for $n_{coll} = n_b$, the luminosity, Eq. (1), grows as the square of n_{coll}. Thus, multiple collisions ease the detrimental effect of beamstrahlung.

Equation (1) shows that the highest luminosity is obtained for the largest value of the product $(n_{coll} n_b N_b^2)$. Maximum luminosity is attained for 'all-beam' collisions, by which we mean each linac bunch collides with each bunch of the other beam. Due to collective effects and beam-optical constraints, the limit of all-beam collisions is

difficult to attain. We will consider two different approaches towards this limit. In the first scheme ('cluster collisions'), every 12 linac bunches are combined into 1 superbunch of $N_b \approx 4.5 \times 10^9$ particles, which is collided head-on with an equivalent superbunch in the other beam. If these superbunches were to collide without charge compensation, an electron (or positron) on average would radiate about 10 photons during a collision, resulting in an induced mean energy loss close to 100%. Thus neutral beams are helpful here. In the second scheme ('multiplexed collisions'), each of the individual linac bunches, with $N_b \approx 3.8 \times 10^8$, is collided with all bunches of the opposing beam by means of a crossing angle. In the absence of charge compensation, an electron would radiate about 2 photons during a single collision, and the average energy loss per collision, δ_b^{coll}, would be about 44%. Evidently, charge compensation is worthwhile for either case, cluster or multiplexed collisions.

Table 1 shows two sets of interaction-point beam parameters for a 5-TeV W-band collider, corresponding to the two schemes outlined above. Assuming the same number of 25 electron and 25 positron bunches in the two linacs, the total luminosity is about 5×10^{34} cm^{-2}s^{-1} for cluster collisions, and twice this number, *i.e.*, 10^{35} cm^{-2}s^{-1}, in the case of multiplexed collisions. Thanks to the multiple collisions, this luminosity is achieved with a rather small average beam power of less than 1 MW per side. Emittances, charge and bunch length are chosen such that the (electron) bunches could be produced by an advanced rf gun. Since the two transverse design emittances are assumed to be the same, the interaction-point spot size is taken to be round, in both planes limited by the Oide effect. The 30-μm rms bunch length is chosen somewhat arbitrarily to be about 1% of the rf wavelength. For shorter bunches the resistive-wall wakefield in the 91-GHz accelerating structures can become significant.

1.3. *Outline*

Section 2 describes the generic final-focus layout, which applies to either one of the two collision schemes. Section 3 is devoted to specific details of the cluster collisions. In Section 4, we discuss the multiplexed collisions. The paper concludes, in Section 5, with a short summary, a discussion of difficulties in the two approaches, and a short outlook on future studies.

2. Generic Layout of the Final Focus

In this section, we first discuss the length scaling with energy of a conventional final-focus system, demonstrating the need for a new paradigm. Abandoning the conventional design philosophy, we then put forward a compact final-focus system for a 5-TeV linear collider. Subsequently, we discuss a variety of design features, including the chromatic bandwidth of the proposed optics, the energy spread that can be achieved with harmonic acceleration, an electron-positron combiner for charge compensation and the importance of the Oide effect.

Table 1. IP beam parameters for a W-band linear collider. The abbreviation 'neutr.' stands for neutralization, *i.e.*, charge compensation.

parameter	symbol	scheme I: cluster collision	scheme II: multiplexing
beam energy	E	2.5 TeV	
charge per bunch at IP	Q	720 pC	60 pC
particles per bunch	N_b	4.5×10^9	3.75×10^8
number of equal-charge bunches per pulse	n_b	2	25
number of collisions per bunch	n_{coll}	1	25
number of species per bunch ($n_{pair} = 2$ means neutralization)	n_{pair}	1 or 2	2
hor. bunch separation in linac	Δx	1.4 mm	
bunch-to-bunch time separation	Δt	300 ps	20 ps
longitudinal bunch spacing	L_{sep}	9 cm	6 mm
repetition frequency	f_{rep}	120 Hz	
average beam power (per side)	P	0.7 MW	
rms bunch length	σ_z	30 μm	
rms intrabunch energy spread	δ_{rms}	10^{-5}	
horizontal emittance	$\gamma\epsilon_x$	100 nm	
vertical emittance	$\gamma\epsilon_y$	100 nm	
hor. IP spot size	σ_x	1.7 nm	
vert. IP spot size	σ_y	1.7 nm	
hor. IP divergence	θ_x	11.5 μrad	
vert. IP divergence	θ_y	11.5 μrad	
hor. IP beta function	β_x^*	150 μm	
vert. IP beta function	β_y^*	150 μm	
average linac beta function	$\beta_{x,y}^{linac}$	25 m	
disruption parameter/collision w/o neutr.	$D_{x,y}$	26.2	2.2
beamstr. parameter w/o neutr.	Υ	200	16
beamstr. no. of photons/electron /collision w/o neutr.	N_γ	9.8	1.8
beamstrahlung average energy loss /collision w/o neutr.	δ_b^{coll}	'100%'	44.0%
total luminosity w/o pinch & w/o Oide effect & w. neutr.	L_{tot}	5×10^{34} cm^{-2} s^{-1}	10^{35} cm^{-2} s^{-1}

2.1. *Length Scaling for a Conventional Final Focus*

At TeV energies, synchrotron radiation in the bending magnets, conventionally introduced for chromatic correction, is prone to cause significant emittance growth. This emittance growth can only be reduced to a reasonable level by using very weak bending magnets. Unfortunately, for a 5-TeV collider this would require a system length of many kilometers. The length optimization of a final focus was discussed previously.[4] In the following we present a simplified summary.

Chromatic correction conventionally is achieved by placing sextupole magnets at a location with large dispersion. Typically, the sextupoles are arranged in pairs, so that they are separated by an optical $-I$ transform to suppress aberrations. There often is one pair correcting the horizontal chromaticity and a second pair correcting the vertical chromaticity. In a symmetric design, the dispersion at the two sextupoles of a pair is determined by the bending magnets situated between them. Bending magnets must also be installed before and after these sextupoles, in order to match the dispersion to zero on both ends. The additional rms energy spread induced by synchrotron radiation in the bending magnets scales as

$$(\Delta\delta_{rms})^2 \propto \gamma^5 \frac{\theta_B^3}{l^2} \tag{5}$$

where θ_B denotes a characteristic bending angle, *e.g.* the total angle between the two main sextupoles in the vertical chromatic correction section (CCY), and l is the final-focus length. The energy spread ($\Delta\delta_{rms}$) generated inside and behind the CCY is not chromatically corrected. It thus increases the IP spot size by interacting with the uncompensated vertical chromaticity of the final doublet ξ_y. In order to restrict this blow up to less than 40%, we must require that

$$\xi_y \ \Delta\delta_{rms} \ll 1. \tag{6}$$

If we assume that in going to higher energies the free length between the interaction point and the last quadrupole as well as the normalized beam emittances are held constant, and that the luminosity increases as γ^2, the vertical chromaticity must increase at least in proportion to the beam energy:

$$\xi_y \propto 1/\beta_y^* \propto \gamma. \tag{7}$$

The sextupole strength is chosen so as to correct the chromaticity of the final doublet, a condition which can be written

$$2\eta_{SY} \ (k_{SY} l_{SY})\beta_{SY,y} \approx \xi_y, \tag{8}$$

where η_{SY} and $\beta_{SY,y}$ denote the dispersion and vertical beta function at the two vertically correcting sextupoles. The term $(k_{SY} l_{SY})$ is the integrated sextupole strength. The dispersion at the sextupoles, η_{SY} in Eq. (8), is proportional to the product of bending angle and system length:

$$\eta_{SY} \propto \theta_B l. \tag{9}$$

Orbit perturbations which are generated inside the chromatic correction section and which thus alter the orbit at only the second quadrupole of a pair can strongly affect the IP beam size. A horizontal orbit change at the second sextupole by an amount Δ due to such an internal perturbation moves the longitudinal location of the beam waist at the IP, and thereby increases the spot size at the collision point. This sensitivity to horizontal orbit variations translates into a limit on the product $(k_{SY} l_{SY})\, \beta_{SY,y}$, which reads

$$(k_{SY} l_{SY})\, \beta_{SY,y} \leq \frac{1}{\Delta}. \tag{10}$$

The limit of Eq. (10) corresponds to a 40% luminosity loss. If we assume that the achievable value of Δ cannot be improved much beyond the value required for the NLC, the combination of Eqs. (5)–(10) yields the scaling law

$$l \propto \gamma^2. \tag{11}$$

So, we expect that the final-focus length increases roughly as the 2nd power of energy!

Figure 4 illustrates the dependence of length and orbit sensitivity on beam energy for 5 actual collider designs: the final focus of the Stanford Linear Collider (SLC),[5,6] the Final Focus Test Beam (FFTB),[7] the TESLA linear collider,[8] the Japan Linear Collider (JLC),[9] and the Next Linear Collider (NLC).[10] These systems were designed to operate at different beam energies between 50 GeV and 750 GeV, and, thus, provide illustrative data points. The figure shows that, consistent with our assumption, the sensitivity Δ varies at most by a factor of a few, independent of energy. However, the increase with length is weaker than predicted. The likely reason for this scaling violation is that the length of the lower-energy systems, FFTB and SLC, is not dictated by the bending magnets. In these two machines bending magnets are found only in a small fraction, about 10%, of the total final-focus length. This is in contrast to the NLC, where the bends occupy more than 50% of the space.

As an example, the length of the NLC final focus, whose sextupole-orbit sensitivity Δ is 500 nm and which was designed for a maximum beam energy of 750 GeV, is almost 2 km per side.[10] The preceding collimation and diagnostics sections on either side are an additional 3 km long. Extrapolating to higher beam energies, we find that at 2.5 TeV the total length of the final focus alone will exceed 40 km, if scaled quadratically (20 km, if linearly). This length figure can in principle be reduced by changing other machine parameters: charge per bunch, repetition rate, normalized emittance, and so on, but the trend is clear and unsettling. With such a final-focus paradigm one is led to question the value of a compact, high-gradient linac to future high-energy physics machines.

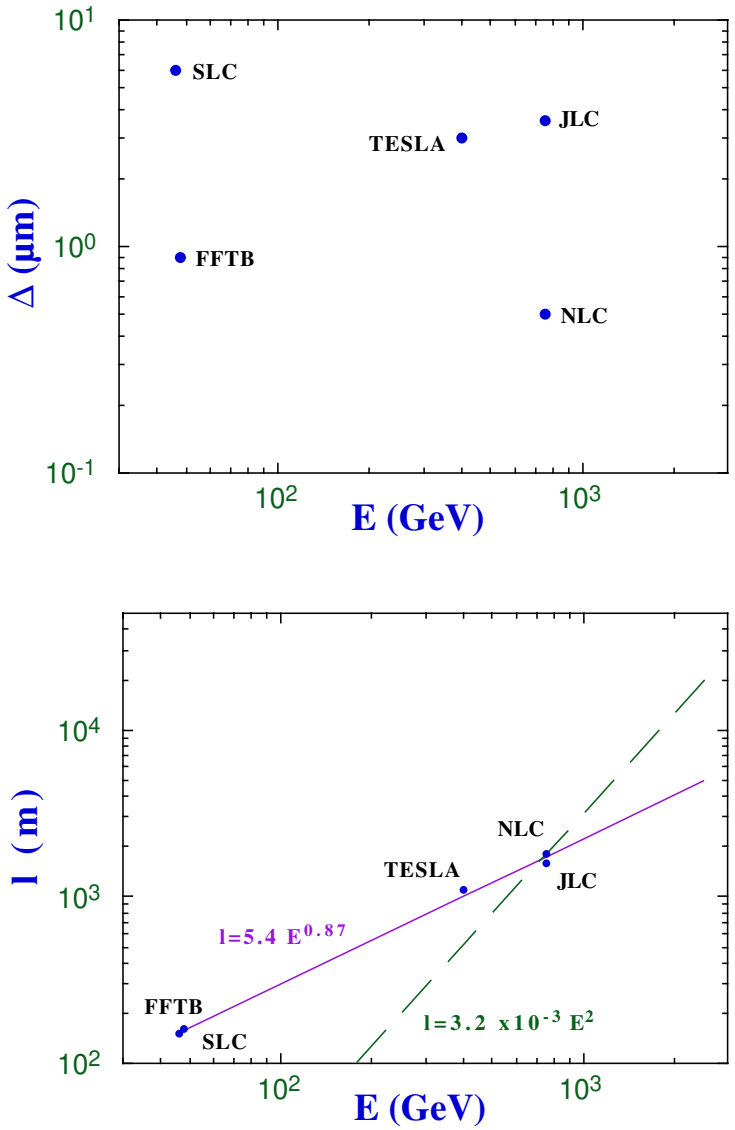

Fig. 4. Energy scalings exemplified by 5 different final-focus designs: (top) orbit-sextupole sensitivity Δ vs. beam energy; (bottom) system length vs. beam energy.

2.2. *Compact Final Focus*

In view of the above scalings, it appears next to impossible to extend the conventional concept of a final-focus system to ever higher energies. The enormous final-focus lengths required would not only appear impractical but also mitigate the benefits of a compact linac. We therefore embark on a different approach and completely abandon any chromatic correction, by confining the chromaticity and by keeping the intrabunch energy spread sufficiently small, so that the uncorrected chromatic spot-size increase is still tolerable. Indeed this approach is quite natural, since there is a large imbalance between the emittances of the three planes of motion. Surprisingly, in most collider designs so far no emphasis is placed on a reduction of the longitudinal beam emittance, while the transverse and, in particular, the vertical emittances are pushed to ever more extreme values.

A final focus without sextupoles also relieves most of the tolerances on magnet positions and field stability. The tight alignment and stability tolerances for typically 100 magnets in a conventional chromatic correction section are replaced by the tolerance for a single parameter: the intra-bunch energy spread. The latter should be much easier to control and to correct.

Since the beams are round at the IP, we conceive the final focusing lens as a triplet, consisting of 3 quadrupoles. These quadrupoles might be conceived as rf quadrupoles, integrated into the W-band matrix accelerator, or they could be small-aperture permanent magnets. We assume that the maximum pole-tip field of a permanent quadrupole magnet, or the equivalent field value of an rf quadrupole, is on the order of 1 T. The free length from the IP l^*, the quadrupole aperture a_q and the stay-clear (expressed as a multiple n of the rms beam size) are related by

$$a_q \geq n\ \theta^*_{x,y} l^*. \tag{12}$$

As an example, with an aperture a_q of 100 μm and a 1-T pole-tip field, the strength of the last quadrupole is $K_{quad} \equiv B_T/(a_q(B\rho)) \approx 1\ \mathrm{m}^{-2}$, where $(B\rho)$ denotes the magnetic rigidity. The corresponding field gradient is 10 kT/m. For an rms beam divergence $\theta_* \approx 11$ μrad, and a free length l^* of 2 m, the beam stay-clear is not much larger than 4σ. We would prefer at least 10σ. In the case of cluster collisions, where the exiting beam may have to pass through the same magnet apertures as the incoming one, a 4σ stay-clear would be problematic. Fortunately, in this case the transverse separation of the two collision points is quite large, and a high-gradient superconducting quadrupole with a larger bore, providing up to 25σ beam stay-clear, could be employed. Also in the case of multiplexed collisions, a larger stay-clear can be obtained by reducing l^*.

Figure 5 depicts a final-focus optics for a 2.5-TeV W-band collider based on the above parameters. The total length of this final-focus system is about 270 m. In the beamline schematic on top, the large open rectangles of 140 m total length represent a vertical half-chicance, that is used for combining electron and positron bunches into neutral beams (see Subsection 2.5). Just upstream of the dipoles, the horizontal beta function is reasonably large and the electron and positron beams

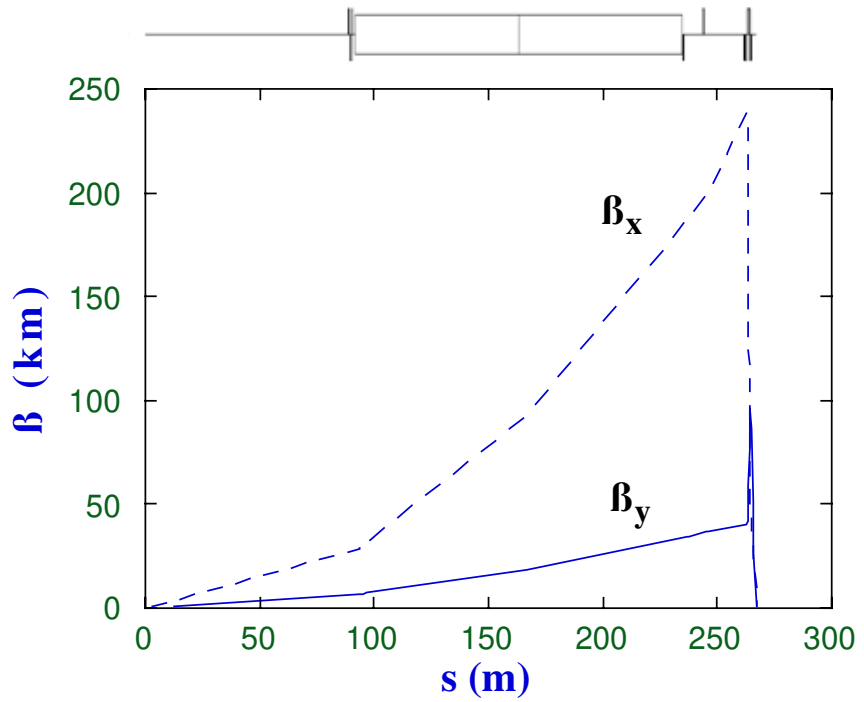

Fig. 5. Final-focus optics for a W-band linear collider, with a total length of 270 m. The IP is on the right in this figure.

are still separated. This would be the ideal location for a crab cavity if the beams are to be collided under a crossing angle (compare the discussion on crossing angle and crab cavities in Section 4).

2.3. *Chromatic Bandwidth*

The chromaticity of the final focus is to a large extent determined by the final triplet, inside which the beta functions are of the order $\beta_{x,y}^{quad} \approx 200$ km, as seen in Fig. 5. Considering one quadrupole (the chromaticities of focusing and defocusing quadrupoles partially cancel) of length $l_{quad} \approx 0.5$ m, and strength $K_{quad} \approx 1$ m^{-2}, the chromaticity is roughly $\xi_{x,y} \approx \beta_{x,y}^{quad} (Kl)_{quad} \approx 10^5$. If this chromaticity is uncompensated, it causes a relative spot-size increase of

$$\frac{\Delta\sigma_{x,y}}{\sigma_{y0}} \approx \xi_{x,y}\delta_{rms}, \tag{13}$$

to be added in quadrature, where σ_{y0} ($\sigma_{y0} \approx \sigma_{x0}$) is the unperturbed design spot size, $\xi_{x(y)}$ the horizontal (vertical) chromaticity, and δ_{rms} the intrabunch rms energy spread. A multiparticle tracking simulation shows that an rms energy spread of $\delta_{rms} \approx 10^{-5}$ results in a spot-size increase of about 10%, as seen in Fig. 6.

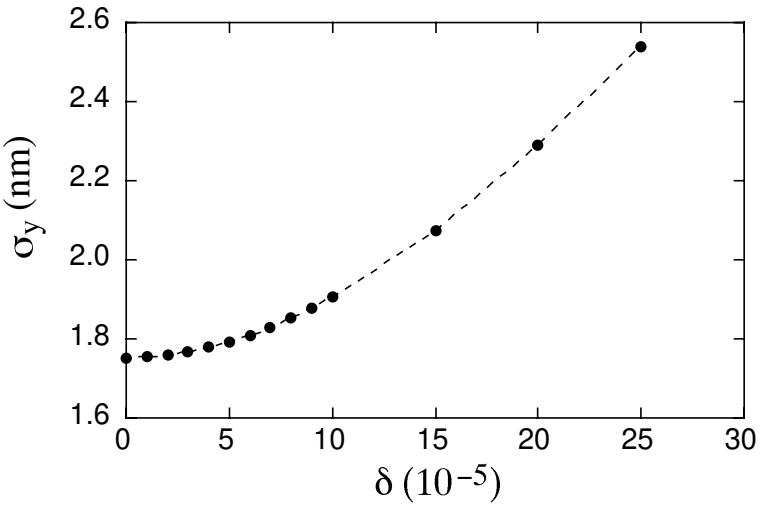

Fig. 6. Energy bandwidth for the final-focus optics of Fig. 5, as obtained from a tracking simulation with the program MAD.[11]

2.4. *Harmonic Acceleration*

As discussed in the previous section, without sextupole correction the control of the chromatic spot-size increase requires a very small energy spread across each bunch. We may attain this energy spread by employing rf acceleration sections operated at harmonics of the fundamental. The energy kick imparted by a linac with harmonic acceleration and single-bunch beam loading takes the form

$$V(t) = \sum_h V_h \cos(h\omega_1 t + \phi_h) - \int^t dt'\ I(t') W_\parallel (t - t'), \tag{14}$$

with V_h, ϕ_h the voltage and phase for the harmonic h, and ω_1 the angular frequency for the fundamental. The function $W_\parallel$ describes the longitudinal wakefield of the linac and $I > 0$ the bunch current waveform. For the sake of definiteness let us consider a model wakefield, varying with time as $W_\parallel \propto t^{-\nu}$, and a 'flat-top' current profile turning on at $t = 0$ and extending to $t = T$, with total charge Q.

For the case of a single harmonic, the fundamental voltage and the wakefield may be expressed as

$$V_L(t) = \cos(\omega_1 t + \phi) - \int^t dt'\ I(t') W_\parallel (t - t'), \tag{15}$$

the total voltage is

$$V(t) = V_L(t) + V_h \cos(h\omega_1 t + \phi_h). \tag{16}$$

We wish to select the amplitude and phase of the harmonic rf, V_h and ϕ_h, such that

the rms voltage is minimized. In terms of

$$\delta V(t) = V(t) - < V >, \qquad \delta E = e^{ih\omega_1 t} - < e^{ih\omega_1 t} > \equiv \delta C + i\delta S \tag{17}$$

one may express the optimal phase as

$$\phi_h = \tan^{-1} \frac{\mathrm{Im}(< \delta V \ \delta E >< \delta C \ \delta E^* >)}{\mathrm{Im}(< \delta V \ \delta E >< \delta S \ \delta E^* >)} \tag{18}$$

and the amplitude as

$$V_h = -\frac{< \delta V \ \delta C >}{< \delta C^2 >}. \tag{19}$$

This is approximately $V_h/V_1 \approx -1/h^2$. In Eqs. (17)—(19), $< ... >$ denotes an average over the bunch, and δC and δS are the real and imaginary parts of δE, respectively.

As an example, we take $\nu = 0.5$ and $h = 10$. In this case, by optimizing the three parameters: fundamental mode phase, harmonic phase and harmonic amplitude, it is possible to achieve an rms energy spread of 1.6×10^{-4} with a normalized harmonic amplitude of 1.2×10^{-2}. If one excludes the front 5% of the beam, the energy spread drops to 3.9×10^{-5}; excluding the front 10% it is only 1.4×10^{-5}, close to the required value. Adding a third frequency ($h' \approx 30$), and optimizing its phase and amplitude as well, the energy spread can be further reduced to 9×10^{-6} excluding the front 5% of the beam, and to 2.5×10^{-6} excluding the front 10%. Figure 7 compares the loaded and unloaded waveforms that can be attained in a conventional single-frequency linac with those for a two and three frequency linac.

The total rf input energy per pulse for all harmonic sections together as a fraction of that for the fundamental mode rf system is

$$\frac{U_h}{U_1} \approx \frac{1}{\rho h^4} \tag{20}$$

where ρ is the fractional contribution to the loss factor from the harmonic sections. For $h = 10$ and $\rho = 10\%$, $U_h/U_1 \approx 10^{-3}$. This corresponds to a field of 200 MeV/m at 0.91 THz, and a 5% reduction in average gradient due to the additional length of the harmonic sections.

2.5. *Charge Compensator*

The layout of the switched matrix accelerator can be arranged such that electron and positron bunches are copropagating in parallel channels, which are separated vertically by about 3 mm, as illustrated in Fig. 1. In the final focus, the pairs of co-propagating bunches can then be combined into single neutral bunches. As stated before, the motivation for this charge compensation is to reduce the energy loss due to beamstrahlung.[1]

The combination of electron and positron bunches is accomplished using a magnetic half-chicane, consisting of two successive vertical bending magnets, each of length l_0 and with opposite deflection angles $\pm\theta$ and bending radii $\pm\rho = \pm l_0/\theta$.

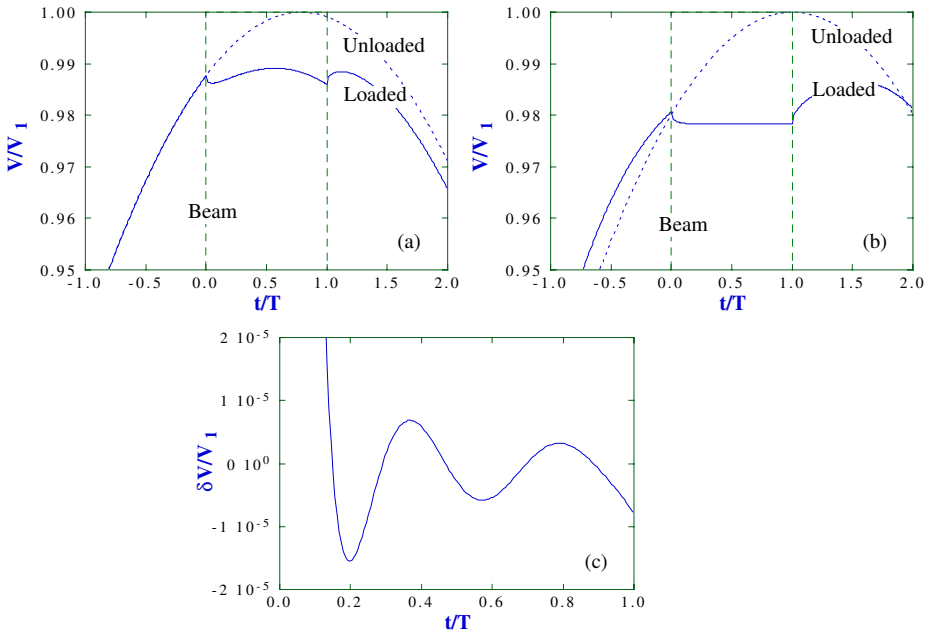

Fig. 7. Loaded and unloaded voltage waveforms for a wakefield parameter $\nu = 0.5$: (a) in a conventional single frequency linac, with a total rms energy spread of $\delta_{rms} \approx 10^{-3}$; (b) in a two frequency linac, with $\delta_{rms} \approx 1.6 \times 10^{-4}$; (c) in a three frequency linac, with $\delta_{rms} \approx 2.5 \times 10^{-6}$ excluding the first 10% of the beam (shown here is the difference from the average voltage; note the magnified scale).

If the initial vertical separation of the electron and positron bunches is Δy, the condition for beam combining in the half-chicane is

$$\frac{1}{4}\,\Delta y = \rho - \sqrt{\rho^2 - l_0^2} \approx \frac{l_0^2}{2\rho} \approx \frac{l_0\theta}{2}. \tag{21}$$

The miminum length of the bending magnets is determined by the emittance growth due to synchrotron radiation, an effect which was analyzed by Sands,[12] Crosbie[13] and Spence,[14] and by the induced energy spread. In the limit of many photons ($\theta\alpha\gamma \gg 1$; with $\alpha \approx 1/137$ the fine structure constant), the emittance at the end of the half chicane (for zero initial emittance) is

$$\epsilon_r = \frac{55\ \sqrt{7}}{144\ \sqrt{3}} \frac{r_e^2}{\alpha}\ \left(\frac{\gamma}{\rho}\right)^5\ l_0^4. \tag{22}$$

For $\gamma = 5 \times 10^6$ this amounts to

$$\gamma\epsilon_r \approx 10^{-17}\ \text{m rad}\ \frac{\theta[\mu\text{rad}]^5}{l_0[\text{m}]}. \tag{23}$$

If we restrict the emittance growth to a value not larger than $\gamma\epsilon_r \leq 10^{-8}$ m rad

(one tenth of the incoming beam emittance), the minimum half length is given by

$$l_0 \geq 1.8 \times 10^3 \ (\Delta y[\mathrm{m}])^{5/6}. \tag{24}$$

A second constraint on the length arises more directly from the induced energy spread, given by[12]

$$\delta_{rms}^2 = \left(\frac{55 r_e \lambda\!\!\!^{-}_c}{12\sqrt{3}}\right) \frac{\gamma^5 \theta^3}{l_0^2} \tag{25}$$

where r_e is the classical electron radius and $\lambda\!\!\!^{-}_c$ the Compton wavelength. If we require $\delta_{rms} \leq 5 \times 10^{-6}$, combining Eqs. (21) and (25) yields

$$l_0[\mathrm{m}] \geq 2.1 \times 10^3 \ (\Delta y[\mathrm{m}])^{3/5}. \tag{26}$$

For $\Delta y \approx \lambda_{rf} \approx 3.3$ mm, the first limit, Eq. (24), amounts to $l_0 \geq 15$ m, while the second limit, Eq. (26), implies the more stringent condition $l_0 \geq 70$ m. The corresponding bend angle is $\theta \leq 24$ μrad. In the optics design of Fig. 5, we have included a half-chicane combiner consisting of two 70-m long bending magnets. The momentum compaction factor of the half-chicane is $R_{56} = -\frac{2}{3}\theta^2 l_0 \approx 26$ nm, with negligible effect on the IP bunch length.

Charge compensation imposes stringent tolerances on accelerator and magnets. For example, if the centroid energy of a bunch differs from the nominal value, or if the field of the combiner bending magnet fluctuates, the overlap of the two oppositely charged bunches is not perfect. Allowing for a maximum centroid-to-centroid offset of the combined electron and positron bunches that is equal to 0.5% of the rms beam size (the latter is 14 μm at the combiner), the tolerance on the energy and field stability is 0.01%.

If the two bunches are initially offset with respect to one another, a charge-separation instability develops.[1,2] For a single collision point, this effect was analysed previously, both analytically and by a computer simulation.[15] The growth of the offset per collision is a function of only one parameter, $A \equiv (4D/\pi)^{1/2}$, where D denotes the disruption parameter for the plane under consideration in the absence of neutralization,

$$D_{x,y} \equiv \frac{2N_b r_e}{\gamma} \frac{\sigma_z}{\sigma_{x,y}(\sigma_x + \sigma_y)}. \tag{27}$$

An initial offset of two co-propagating beams by 2Δ, per collision gets amplified by a factor

$$\frac{\Delta^{out}}{\Delta^{in}} \approx \frac{e^A}{2\sqrt{2\pi}\sqrt{A}} \qquad \text{for } A \gg 1. \tag{28}$$

For the collision of charge-combined superbunches (cluster collisions), this factor is about 200. In the case of multiplexed collisions with a crossing angle, $D \approx 2.2$ and $A \approx 1.67$, and the growth must be computed numerically. The amplification in this latter case is found to be 1.12 per collision, or $1.12^{25} \approx 17$ for 25 successive collisions. This shows that for multiplexed collisions, where charge compensation is more essential, the charge-separation instability is less severe. An external focusing between the collision points can further reduce the remaining sensitivity.

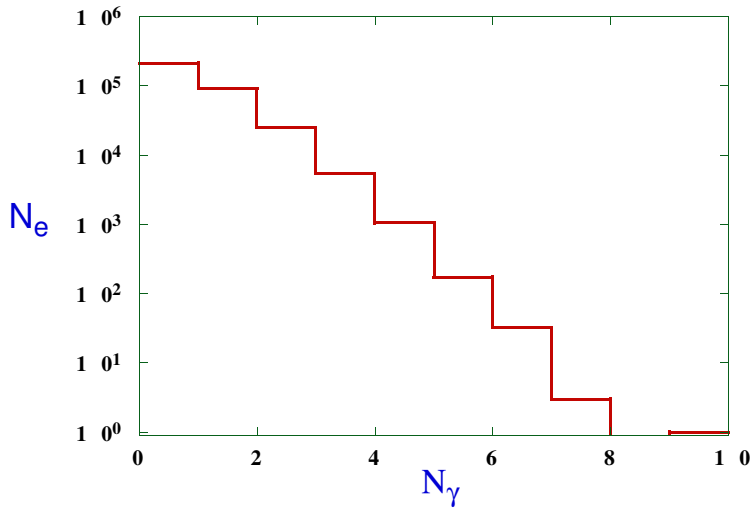

Fig. 8. Histogram of number of photons emitted per electron in the final doublet. The first bin corresponds to 0 photons radiated. The total number of electrons sampled in the simulation was $N \approx 3.3 \times 10^5$.

2.6. *Oide Limit*

The spot-size increase due to synchrotron radiation in the final focusing lens was first studied by Oide.[16] Due to the statistical character of the photon emission and the resulting non-Gaussian distribution, the actual luminosity loss will be considerably smaller than that calculated from the rms spot-size increase.[17] To study the Oide effect for the last quadrupole in our W-band final focus, we have written a Monte Carlo simulation. The simulation results show that on average 0.48 photons are emitted per electron with an average relative energy decrement of 5×10^{-5}. The resulting 'core' rms beam sizes at the IP (where the 'core' is defined by the exclusion of fliers beyond 9σ) are 2.5 nm in both planes, and the luminosity is about 20% lower than the nominal luminosity without synchrotron radiation.

Typical results of the Monte Carlo simulation are depicted in Figs. 8, 9 and 10. Figure 8 shows the distribution of the photons emitted per electron. In Fig. 9, we present the rms beam sizes, both including and excluding particles outside 9σ, as a function of the initial normalized beam emittance. Figure 10 shows the relative luminosity loss, also as a function of the emittance. For normalized emittances larger than the design value of 10^{-7} m-rad, the luminosity decreases strongly.

3. Cluster Collisions

The cluster-collision scheme is illustrated by a schematic in Fig. 11. This scheme requires the combination of every 12 electron or positron bunches into one superbunch. The electron and positron superbunches thus produced are (optionally) combined to form neutral superbunches, using the vertical half-chicane discussed

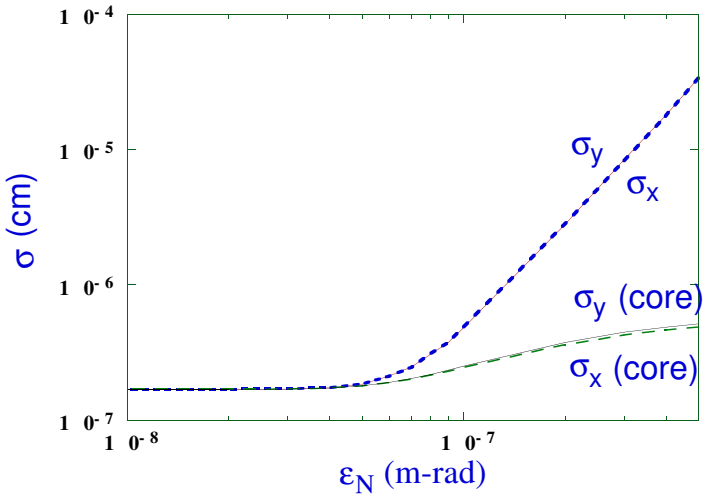

Fig. 9. Variation of the rms IP beam sizes and the rms 'core' beam sizes at the first IP focal point (the 'core' is obtained by removing fliers outside $\pm 9\sigma$) versus the normalized beam emittance.

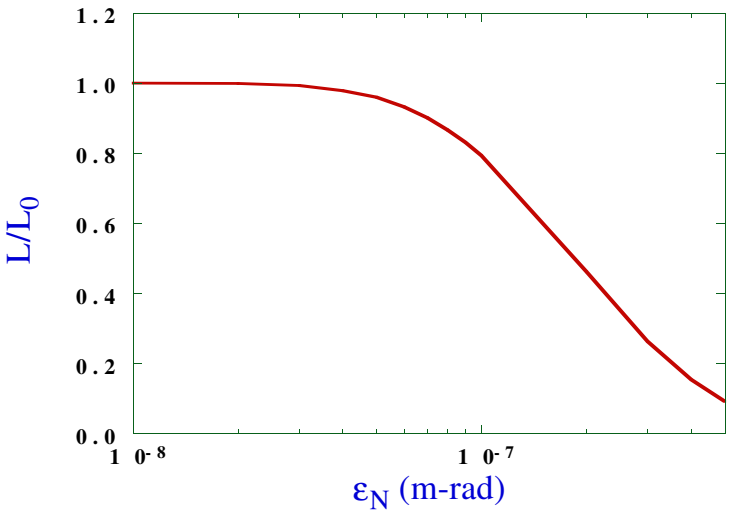

Fig. 10. Relative luminosity reduction at the first IP focal point due to the Oide effect versus the normalized beam emittance. Luminosity is computed using area-weighted charge allocation on a Cartesian grid.

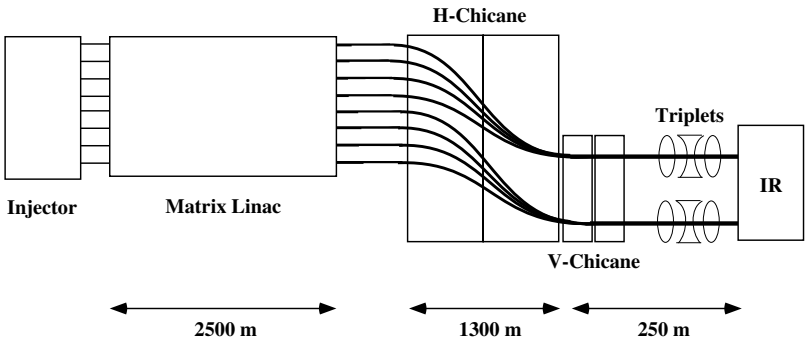

Fig. 11. Schematic (not to scale) of a W-band final focus combining groups of 12 bunches into superbunches, which are charge-compensated and collided head-on ('cluster collisions'). There is one common interaction point for every 12 linac bunches.

above. The superbunches are collided head-on in a single collision with an equivalent superbunch of the opposing train.

3.1. *Half-Chicane Combiner with Dispersion and Energy Slew*

The challenge in this scheme is the production of the superbunch. One possibility is the use of a horizontal half-chicane. Since the 12 bunches all have the same sign of charge, we must introduce an energy variation from bunch to bunch and utilize the nonzero dispersion at the end of the chicane to combine them. The combination condition reads

$$\Delta x = 2\,\frac{l_0^2}{\rho}\,\Delta\delta \tag{29}$$

where Δx is the inter-channel distance, l_0 the length of one bending magnet (half the half-chicane), ρ the bending radius and $\Delta\delta$ refers to the bunch-to-bunch energy difference. The emittance growth and energy spread induced by synchrotron radiation are again given by Eqs. (23) and (25), respectively. The minimum length required for $\gamma\epsilon_r \leq 10^{-8}$ m-rad and $\delta_{rms} \leq 5\times 10^{-6}$ is obtained by replacing in Eqs. (24) and (26) the vertical displacement Δy with the horizontal interchannel spacing divided by the energy difference, $(\Delta x/\Delta\delta)$.

Suppose now that the bunch-to-bunch energy difference $\Delta\delta$ is 1%, so that the total energy variation across a group of 12 bunches is 12%. Then, for an interchannel spacing Δx of 1.4 mm, the minimum length of the horizontal half-chicane is $2l_0 \geq$ 1300 m and the half bending angle θ is about 100 μrad. The dispersion at the end of the horizontal half chicane is

$$\eta_f \approx 2\theta l_0 \approx 14 \ \text{ cm}. \tag{30}$$

Since the rms beam size at this point is about 20 μm and the relative intra-bunch

energy spread does not exceed 10^{-5}, this dispersion, if uncompensated, would increase the beam size by less than 10%. Also the centroid energy of each bunch must be controlled and maintained at the 10^{-5} level, a stringent requirement. The inter-bunch energy variation is not a problem per se, since the beta functions for each bunch energy can be adjusted independently at the end of the linac; a challenge of off-energy matching.

3.2. *Off-Energy Matching*

Two disadvantages of the described cluster-collision scheme are that the charge combiner is 5 times longer than the final focus proper, and that the nominal luminosity is a factor of 2 lower than in the ideal case of 'all-beam collisions.' In order to recover the target luminosity of 10^{35} cm^{-2} s^{-1} at the same rf power figure, the number of bunches would have to be doubled, to 2 batches of 2×24 electron and positron bunches each. This would raise the pulsed heat load on the linac and it is yet unclear that this would be acceptable. A third complication is the need to individually match the linac optics of each channel so as to obtain the same spot size at the interaction point for largely differing beam energies. This matching can be accomplished by means of individual quadrupole magnets in the still separated beam lines, and, thus, it differs from conventional chromatic correction in that it requires neither sextupoles nor bending magnets.

Figure 12 illustrates the beta functions across the final triplet for three different beam energies, covering a total energy range of 10%. In principle, the optics at the end of the linac, prior to the charge combiner, can be adjusted to match into the correct off-energy beta functions at the triplet. In practice, this could be difficult as this may imply an unrealistically large beam size at the entrance to the combiner. Thus, the requirements posed by a simultaneous multi-energy match will likely require modifications of the final focus optics depicted in Fig. 5. For example, a continuous lattice of moderately strong quadrupoles, without large drift spaces, could constrain the off-energy beta functions and be more adaptable to a versatile energy matching.

4. Multiplexed Collisions

As an alternative of the 'cluster' collision scheme of the last section, let us consider next 'multiplexed' collisions of charge-compensated bunches, realized by means of a crossing angle. To avoid a large luminosity reduction and instabilities due to the crossing angle, crab cavities[18] rotate the bunches so as to establish head-on collisions. A schematic of the overall layout is depicted in Fig. 13. Figure 14 provides a close-up view of the IP collisions.

The advantages of this scheme are that the inter-bunch energy variation can be zero, thus avoiding the serious matching difficulties which a large energy variation entails. In addition, without the horizontal combiner, the length of the final-focus system is much reduced. Moreover the luminosity, for the same number of bunches,

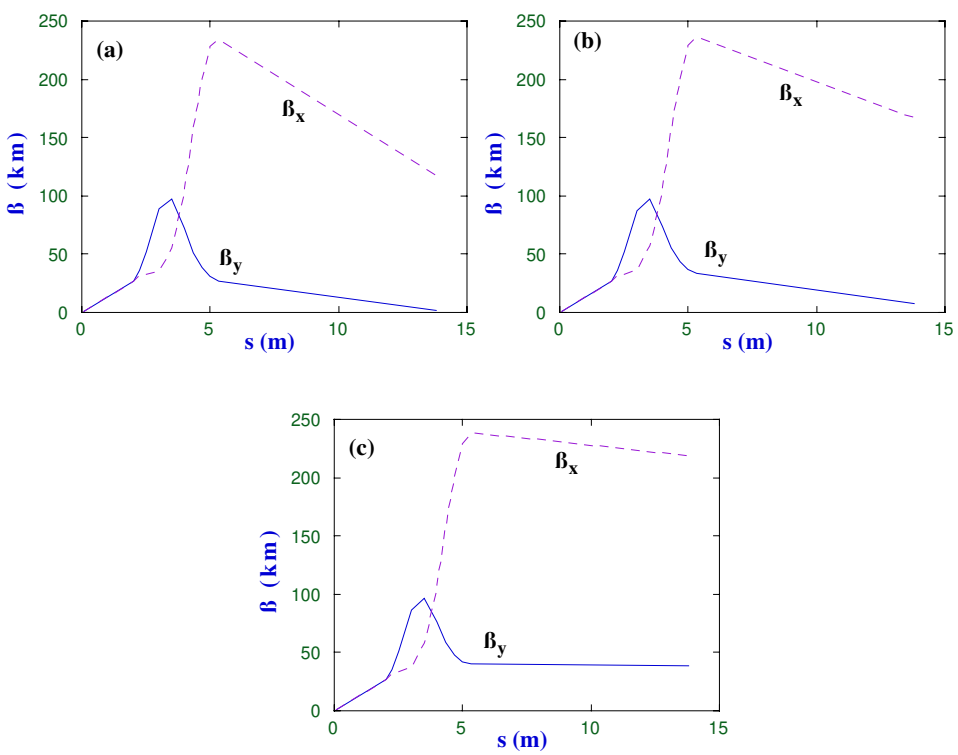

Fig. 12. Horizontal and vertical beta functions calculated from the interaction point backwards through the final triplet for an energy deviation relative to the design optics of (a) -10%, (b) -5%, and (c) 0%. The IP beta functions are held constant at $\beta^*_{x,y} \approx 150$ μm. The IP is on the left in these figures.

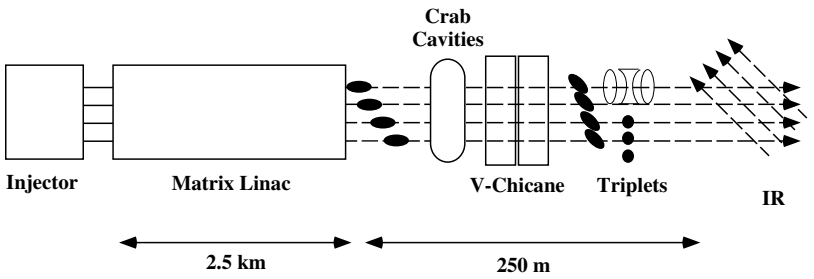

Fig. 13. Schematic (not to scale) of a W-band final focus with multiplexed collisions, crossing angle, crab cavities and charge compensation ('multiplexed collisions').

is higher than in the case of cluster collisions. A serious conceptual disadvantange is the necessity to repeatedly focus each bunch over distances of about 4 mm to the interaction-point spot size. This would require quadrupole fields of unprecedented strength, and cannot be achieved with conventional technologies, if at all.

4.1. *Crossing Angle*

The geometry of the multiplexed collisions with crossing angle is depicted schematically in Fig. 14. The half crossing angle θ is given by

$$\tan\theta = \frac{\Delta x}{L_{sep}} \tag{31}$$

or, inserting the parameters of Table 1, $\theta \approx 230$ mrad (13°). Introducing the rf group velocity (divided by the velocity of light) in the matrix transmission line, β_g, and considering the design assumptions for the matrix linac, the crossing angle is also related to the rf group velocity v_g via

$$\theta \approx \arctan\frac{v_g}{c}. \tag{32}$$

The distance a bunch travels between two successive collisions is

$$s = \frac{L_{sep}}{\sqrt{2}\cos\theta} \approx 4.4 \text{ mm}. \tag{33}$$

This collision-point separation s is, on the one hand, much larger than the bunch length or the IP beta function, on the other hand, short compared with the focal length of typical or conceivable quadrupole magnets. It implies repeated strong focusing over millimeter distances. In Subsection 4.3 we consider different techniques of IP focusing.

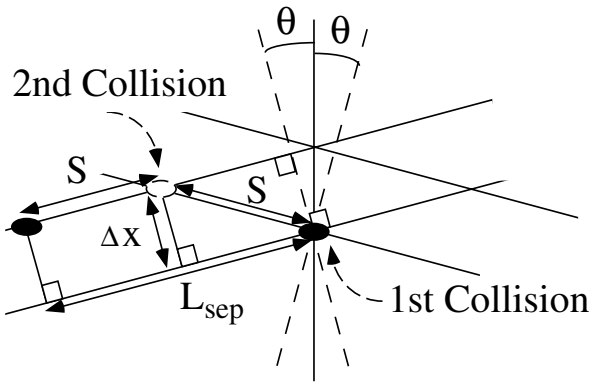

Fig. 14. Multiplexed collisions with a crossing angle.

4.2. *Crab Cavities*

The crab cavities can be located just upstream of the charge-compensating combiner (about 200 m upstream of the interaction point, in Fig. 5; just prior to the charge combiner). The horizontal beta function at this location is $\beta_{CC,x} \approx 25$ km, and the relevant transport matrix element to the interaction point is $R_{12}^{cc\to IP} \approx \sqrt{\beta_{CC,x}\beta_x^*} \approx 2$ m. The crab cavities are excited at a dipole-mode frequency in such a way that the center of the bunch is at the zero of the oscillating rf field. The front and back of the bunch receive kicks in opposite direction, so that at the interaction point the two colliding bunches are parallel and the collision is effectively head-on.

The required net transverse voltage gradient from the crab structures may be determined from

$$\theta = R_{12}^{cc\to IP}\ \frac{e\partial V_c/\partial x}{E}. \tag{34}$$

We find that $(\partial V_c/\partial x) = 2.9$ GV/cm is sufficient. This can be provided by a 5.5-m length of 100 structures of 50 cells each, assuming a wall-Q equal to 70% of the theoretical, and derating the transverse shunt impedance by an additional factor of 2 (for beam ports) to $R_\perp \approx 35$ MV/cm^2/cell. With these parameters, the fill time is less than 1 ns, the peak power per feed is 100 MW and the average rf power for the entire crab section is about 1 kW at the nominal 120 Hz repetition rate. The peak fields are large, on the order of GV/m. Thus the crab rf design will pose challenges similar to those of the linac, if on a smaller scale.

4.3. *IP Focusing*

Multiplexed collisions at mm-wavelengths or longer require either an unrealistically long depth of focus or, continuous focusing within the interaction region. Continuous focusing is difficult to achieve due to large focusing gradients required, of order 10^9 T/m. Permanent magnet focusing appears to be out of the question

due to the 1 T pole-tip field limit. Magnetic focusing with external current drive would likely imply an active plasma lens, with either MA currents or sub-micron features. Beam-driven plasma focusing is problematic due to the need for focusing of both positive and negative charges; alternating gradient plasma focusing schemes are conceivable, but relatively unexplored. These considerations indicate that magnetic focusing is difficult to accomplish and they suggest looking for alternatives. Even though the required duration of the focusing fields is quite short, only 300 ps, pulsed or electromagnetic focusing techniques appear to be out of the question due to the high peak powers required. Thus one is left with the possibility of electrostatic focusing. While at first sight improbable, there is one venue where the required electrostatic fields may be achievable, and this is the crystal channel.

A beam particle is channeled in a solid crystal if its angle of incidence is sufficiently low, namely if it is smaller than the Lindhard critical angle[19] $\Psi_1 = \sqrt{4Ze^2/4\pi\epsilon_0 pvd}$, where Z is the atomic number of the crystal material, v and p the velocity and momentum of the beam particle, and d the atom spacing. As an example, for the $< 111 >$ axial direction in silicon the Lindhard angle is $\Psi_1 \approx 15\ \mu\text{rad}/\sqrt{p[T\text{eV/c}]} \approx 9.5\ \mu$rad, approximately equal to the rms IP beam divergence of Table 1, and the channeling capture probability integrated over the beam (the 'surface transmission') is of the order 50–70%. Larger channeling efficiencies can be attained by crystals of higher atomic numbers.

To assess the viability of crystal-channel focusing, several further studies will be required, including

- the differences in the channeling properties of electrons and positrons,
- the energy loss due to channeling radiation,[20] and
- the radiation damage suffered by an interaction-point crystal and its typical survival time.

5. Conclusions

In this report, we have outlined the design of a final-focus system for a W-band linear collider with a target luminosity of 10^{35} cm^{-2} s^{-1}. We have presented a viable concept, 'cluster collisions', that could achieve 50% of this value. The alternative, 'multiplexed' collisions could achieve the 'all-beam' limit, but requires IP focusing, a problematic concept. The key elements of this final focus are: no chromatic correction, a small energy spread from the linac, charge compensation, and rf or permanent-magnet focusing. Both the use of rf focusing and the short system length would facilitate the integration of the final focus and the W-band linac. The proposed final focus produces nanometer spot sizes at a c.m. energy of 5 TeV, with a physical layout orders of magnitudes smaller than is achievable in the conventional collider paradigm.

We have discussed two collision schemes which could increase the single-collision luminosity of a few times 10^{33} cm^{-2} s^{-1} to the design value of 10^{35} cm^{-2} s^{-1}:

(1) combining the linac bunches into a few superbunches, which are collided head on, and (2) establishing multiple collisions by means of a crossing angle. Both collision schemes increase the luminosity without affecting the average beam power of about 1 MW.

The challenges or difficulties encountered in these two approaches are the following. If, in the cluster-collision scheme, a combination of several bunches into a single superbunch is to be accomplished using dispersion and a bunch-to-bunch energy slew, a separate optics match at the end of the linac is required for bunches of different energies. The primary challenge of multiplexed collisions is the refocusing between successive collision points. The latter seems to imply ultra-high quadrupole gradients, but new techologies and ideas, *e.g.*, the use of crystal channeling, could make this a viable and attractive approach. In particular, it seems interesting to consider a dual purpose crystal, simultaneously acting as a miniature focusing channel and as a compact high-resolution cubic vertex detector.

Future studies should include: (1) an optimization of the multi-bunch off-energy optics matching and an improved quasi-continuous final-focus optics; (2) a detailed analysis of crystal channeling as a tool for focusing the beam between multiple collision points; (3) a tolerance analysis concerning rf phase stability, magnetic-field drifts and magnet vibrations.

Injection schemes for a W-band collider also require serious study. In this connection it is good to realize that for cluster collisions the benefit of the positron beam is exclusively the presumed 'cleanliness' of the collisions, *i.e.*, the clarity of the energy spectrum, and the avoidance of beamstrahlung photons and pair production. The cost for this is quite high: a more complicated accelerator complex, including a positron source driven by an additional electron linac, damping rings and the like. With electrons only, our parameters are not inconsistent with an rf gun, albeit one at an extreme gradient and requiring no doubt an active rf circuit to control cyclic fatigue. Thus, a 5-TeV $e^{\pm}e^{\pm}$ or $e^{-}e^{-}$ collider opens up many interesting possibilities.

6. Acknowledgements

We thank C. Heusch, O. Napoly, T. Raubenheimer, D. Schulte, R. Siemann and K. Yokoya for their encouragement and helpful comments.

References

1. V.E. Balakin and N.A. Solyak, Proc. XIII Int. Conf. on High Energy Accelerators, Novosibirsk, USSR, p. 151 (1986).
2. J.A. Rosenzweig, B. Autin and P. Chen, Proc. 1989 Lake Arrowhead Workshop on Advanced Accelerator Concepts, p. 324 (1989).
3. P. Chen, "Differential Luminosity under Multiphoton Beamstrahlung", Phys. Rev. D 46, p. 1186 (1992).
4. F. Zimmermann, R. Helm, J. Irwin, "Optimization of the NLC Final Focus System", Proc. of the 1995 Particle Accelerator Conference, Dallas, 1995, p. 710 (1995).

5. K.L. Brown, J. Spencer, "Nonlinear Optics for the Final Focus of the Single Pass Collider," 1981 Part. Acc. Conf., Washington D.C., p. 2568 (1981).
6. J.J. Murray, K.L. Brown, T. Fieguth, "The Completed Design of the SLC Final Focus System," 1987 Part. Acc. Conf., Washington D.C., p. 1331 (1987).
7. Final Focus Test Beam: Project Design Report, SLAC–376 (1991).
8. Conceptual Design of a 500 GeV e^+e^- Linear Collider with Integrated X-ray Laser Facility, DESY 1997–048 (1997).
9. JLC Design Study, KEK–REPORT 97–01 (1997).
10. Zeroth-Order Design Report for the Next Linear Collider, SLAC Report 474, LBNL-PUB-5424, UCRL-ID-124161 (1996).
11. H. Grote and C. Iselin, "The MAD Program", CERN/SL/90-13 (1990).
12. M. Sands, "The Physics of Electron Storage Rings", SLAC-121 (1979).
13. E.A. Crosbie, "Effect of Synchrotron Radiation in the Proposed 4 GeV Argonne Microtron", IEEE Trans. Nucl. Sc., NS–30, 3218 (1983).
14. W. Spence, "Phase Space and Synchrotron Radiation Emission in High Energy Electron Transport Lines", unpublished.
15. D.H. Whittum and R.H. Siemann, "Neutral Beam Collisions at 5 TeV", Proc. of IEEE PAC97 Vancouver (to be published).
16. K. Oide, "Synchrotron Radiation Limit on the Focusing of Electron Beams", Phys. Rev. Lett. 61, 1713 (1988).
17. K. Hirata, K. Oide, B. Zotter, "Synchrotron Radiation Limit of the Luminosity in TeV Linear Colliders", Phys. Lett. B224, 437 (1989).
18. R.B. Palmer, "Energy Scaling, Crab Crossing and the Pair Problem", Proc. of the Summer Study on High Energy Physics in the 1990's, Snowmass '88, World Scientific p. 613 (1988).
19. S. Pape Møller, "Crystal Channeling or How to build a '1000 TESLA Magnet' ", Ninth John Adams Memorial Lecture, CERN 94–05 (1994).
20. P. Chen, Z. Huang, R. Ruth, "Channeling Acceleration: A Path to Ultrahigh Energy Colliders", invited talk at the 4th Tamura Symposium on Accelerator Physics, Austin, Texas, SLAC-PUB-95-6814 (1994).